Published in final edited form as:
J Am Chem Soc. 2016 July 13; 138(27): 8497–8504. doi:10.1021/jacs.6b03599.

In-gene Quantification of *O*^{6}-Methylguanine with Elongated Nucleoside Analogues on Gold Nanoprobes

Ioannis A. Trantakis[*], **Arman Nilforoushan**, **Heidi A. Dahlmann**, **Celine K. Stäuble**, and **Shana J. Sturla**[*]
Department of Health Sciences and Technology, ETH Zürich, Schmelzbergstrasse 9, 8092 Zurich, Switzerland

Abstract

Exposure of DNA to chemicals can result in the formation of DNA adducts, a molecular initiating event in genotoxin-induced carcinogenesis. *O*^{6}-Methylguanine (*O*^{6}-MeG) is a highly mutagenic DNA adduct that forms in human genomic DNA upon reaction with methylating agents of dietary, environmental, or endogenous origin. In this work, we report the design and synthesis of novel non-natural nucleoside analogues 1'-β-[1-naphtho[2,3-*d*]imidazol-2(3*H*)-one)]-2'-deoxy-D-ribofuranose and (1'-β-[1-naphtho[2,3-*d*]imidazole]-2'-deoxy-D-ribofuranose and their use for quantifying *O*^{6}-MeG within mutational hotspots of the human KRAS gene. The novel nucleoside analogues were incorporated into oligonucleotides conjugated to gold nanoparticles to comprise a DNA hybridization probe system for detecting *O*^{6}-MeG in a sequence-specific manner on the basis of colorimetric readout of the nanoparticles. The concept described herein is unique in utilizing new nucleoside analogues with elongated hydrophobic surfaces to successfully measure in-gene abundance of *O*^{6}-MeG in mixtures with competing unmodified DNA.

Introduction

DNA is exposed to chemical and environmental insults such as ultraviolet radiation, reactive oxygen species, and alkylating agents. Endogenous and exogenous methylating agents react with and modify DNA nucleobases, producing primarily N^7-methylguanine (N^7-MeG) and *O*^{6}-methylguanine (*O*^{6}-MeG). These adducts are present in DNA isolated from blood cells and various human tissues.1 *O*^{6}-MeG is formed in DNA by SN_1-type methylating agents,2 represented by *N*-nitroso compounds including known human carcinogens present in the environment, diet, and tobacco.3 Endogenous sources of methylation include S-adenosylmethionine4 and endogenous nitrosation products.5,6

The formation of *O*^{6}-MeG is a molecular initiating event leading to carcinogenesis and cytotoxicity. Upon encountering *O*^{6}-MeG, DNA polymerases often preferentially incorporate thymidine.7–9 The resulting mismatch is a substrate for repair; however, the new strand can persist and normal cells harboring *O*^{6}-MeG display a high rate of G→A mutations.10 Additionally, when cancer cells are treated with methylating agents, futile

[*]**Corresponding Authors**: ioannis.trantakis@hest.ethz.ch; sturlas@ethz.ch.
The authors declare no competing financial interest.

Europe PMC Funders Author Manuscripts

cycling of mismatch repair is exploited to induce cytotoxicity.11 G→A mutations have been causally related with the development of tumors in experimental animals treated with methylating carcinogens.12 The observation of frequent G→A transition mutations in KRAS or p53 genes of human colon and lung tumors lacking O^6-MeG–DNA methyltransferase, an enzyme that repairs O^6-MeG in DNA,13 further supports the etiologic involvement of O^6-MeG in colon and lung carcinogenesis, and underscores the value of detecting its presence in tumor-suppressor or tumor-promoter gene sequences as a potential prognostic marker for cancer risk.

Assessing the accumulation of adducts such as O^6-MeG in DNA is a considerable challenge owing to their extremely low occurrence, which is on the order of only tens to thousands per genome.14–17 O^6-MeG has been quantified by ^{32}P-postlabeling,15,17 immunoassay14,18,19 and mass spectrometry,20 wherein the DNA must be completely digested prior to analysis. Therefore it is not possible to assess O^6-MeG abundance in particular genomic loci of interest, such as oncogenes. Furthermore, these methods provide little information regarding the distribution of alkylation events in the genome, needed to characterize causal relationships between adduct occurrence and genetic mutations observed in cancer. Therefore, a major standing goal for DNA adduct detection is direct quantitative sequencing of genes containing DNA adducts.

Several strategies are emerging for determining the location of DNA adducts within the genome. First, ligation-mediated polymerase chain reaction in combination with PAGE was used to map the distribution of DNA lesions within gene sequences.21 This methodology can be used to examine the distribution of single strand breaks22 and alkali labile adducts (e.g. N^7-MeG),23,24 but not to map the distribution of O^6-MeG. Sequencing of DNA with adducts was also achieved by single-molecule real-time sequencing,25 which enables the detection of an adduct on the basis of the slower rate of polymerase-mediated nucleotide incorporation opposite an adduct. More recently, a method based on the enzymatic removal of oxidation adducts followed by the introduction of marker nucleotides at the gapped sites and subsequent PCR amplification and nanopore sequencing was reported.26 Another related approach was based on the combination of DNA glycosylase-mediated excision of specific DNA oxidation adducts with ligase-mediated formation of deletion mutations at the sites of the lesions, which could then be detected by DNA sequencing.27 These strategies represent major conceptual and practical advances, but quantification of adduct abundance remains to be addressed.

An approach that provides a plausible chemical basis for quantitative in-gene detection of DNA alkylation adducts is based on DNA adduct-directed nucleoside probes containing artificial nucleobase surrogates that complement DNA adducts. For example, a method for site-specifically labeling O^6-MeG with fluorescent tags transferred from complementary artificial nucleosides was reported.28 It is not known whether this approach is viable for sensing O^6-MeG in mixtures of targets. With the goal of expanding alkylation adduct recognition, we have devised a class of synthetic nucleosides with mixed aromatic and H-bonding moieties.29–35 The first example was a perimidinone-derived nucleoside (Per, Figure S1) that formed more stable DNA duplexes when paired with O^6-benzylguanine (O^6-BnG) than with G.29 In a recent proof-of-principle study, we demonstrated that coupling

hybridization probes containing Per with gold nanoparticles (AuNPs) allowed for the quantification of the model O^6-alkylG adduct O^6-BnG within a defined, albeit non-biologically relevant, DNA sequence in the presence of excess unmodified DNA strands.36

When hydrophobic perimidinone- and benzimidazole-derived nucleoside analogues (Benzi, BIM, and Peri, Figure S1) were incorporated into oligonucleotides, more stable DNA duplexes were formed when the synthetic bases were placed opposite adducts vs. unmodified bases.30 Ultimately, the larger nucleosides Peri and Per were found to better stabilize O^6-BnG than did smaller analogues.30 Nucleobases with large π surface areas stack more strongly with neighboring bases than their smaller counterparts since they have more area of overlap with neighboring bases, as demonstrated for benzene, naphthalene, and pyrene nucleosides37,38 and size-expanded natural nucleobases.39–42 Structural characterization studies with short duplexes indicated that Per adopts a *syn* conformation and intercalates into the duplex when placed opposite O^6-BnG, whereas opposite G it adopts the *anti* conformation and forms a less stable wobble pair.43 We proposed, therefore, to re-orient the aromatic rings in Per and Peri in order to probe the potential for their elongated surface to improve hybridization performance.

New hydrophobic, elongated adduct-directed nucleoside analogues 1'-β-[1-naphtho[2,3-*d*]imidazol-2(3*H*)-one)]-2'-deoxy-D-ribofuranose (ExBenzi) and (1'-β-[1-naphtho[2,3-*d*]imidazole]-2'-deoxy-D-ribofuranose (ExBIM) (Figure 1) were synthesized and incorporated into oligonucleotides. The modified oligonucleotides formed more stable DNA duplexes when the artificial nucleosides were placed opposite O^6-MeG vs. G. Furthermore, oligonucleotides with ExBenzi and ExBIM were conjugated to AuNPs to create nanoprobes effective for colorimetric detection of O^6-MeG in cancer-related hotspots of the KRAS oncogene. The colorimetric detection of O^6-MeG is based on the distance-dependent color change caused by AuNP aggregation upon recognition of a target nucleic acid by the nanoprobes (Figure 1).

Results and Discussion

Synthesis of elongated nucleoside analogues and oligonucleotides

ExBenzi and ExBIM were designed to explore the influence of elongated nucleobase shape on adduct recognition. ExBenzi is structurally similar to Benzi but is extended by addition of a benzene ring (Figure 1). Likewise, ExBIM is an extended version of BIM.

Phosphoramidites of ExBenzi and ExBIM nucleosides were newly synthesized as substrates for solid phase DNA synthesis (Scheme S1). ExBenzi (**1**) was prepared by heating neat 2,3-diaminonaphthalene and urea,44 while ExBIM (**2**) was prepared by heating 2,3-diaminonaphthalene in formic acid.45,46 The nucleobases **1** and **2** were glycosylated by nucleophilic displacement of chloride from 1-(α)-chloro-3,5-di-*O*-*p*-toluoyl-2-deoxyribose to yield *O*-toluoylated nucleosides, which were deprotected with NaOMe to yield nucleosides **3** and **4**.29,30,34 Protection of the 5'-OH of **3** and **4** was initially attempted using DMTCl, but very low yields of product were obtained. Thus, DMT groups were installed with the more reactive reagent DMT·BF_4 to obtain **5** and **6**.47–49 Finally, phosphoramidites **7** and **8** were formed by alkylating the 3'-OH of **5** and **6** with chlorinated

phosphotidylating reagent.29 These phosphoramidites were incorporated into oligonucleotides by solid-phase DNA synthesis with an automated DNA synthesizer.

Thermal stability of DNA duplexes containing ExBenzi or ExBIM opposite O^6-MeG

The capability of ExBenzi and ExBIM to stabilize DNA duplexes containing a site-specific O^6-MeG modification relative to those containing G was evaluated in DNA duplexes having the sequence of the KRAS gene surrounding codon 12 and codon 13 (Figure 2). The KRAS oncogene is a gene frequently mutated in patients with colorectal cancer and nearly 97% of all KRAS mutations are localized to codons 12 and 13.50 The evaluation studies were performed with 13-mer target oligonucleotides for which the middle base of the target was the middle base of KRAS codon 13. These targets contained at the middle base position either O^6-MeG or G (O^6-MeG_13mer target and G_13mer target respectively, Table S1). Respective complementary probe oligonucleotides contained ExBenzi, ExBIM, or C at the middle base position (ExBenzi_Probe_1, ExBIM_probe_1, C_Probe_1, Table S1).

The stability of DNA duplexes was investigated by measuring their melting temperature (T_m). The duplex containing G:C at the middle position had a T_m of 66.0 °C (Table 1). When O^6-MeG was paired with C, the T_m decreased to 55.2 °C. The diminished stability of this duplex is consistent with previous studies suggesting that O^6-MeG:C adopts a wobble configuration at physiological pH and thus diminished stability could be attributed to the possibility for two instead of three hydrogen bonds.51 Additionally, the higher degree of lipophilicity of O^6-MeG in comparison to G appears to disrupt stacking interactions within both the modified and complementary strands.52 In contrast, when the duplex contained ExBenzi opposite O^6-MeG, the T_m of the duplex was slightly higher than when the duplex contained ExBenzi opposite G (55.0 °C vs 52.0°C, ΔT_m=3.0 °C, Table 1). Similarly, when the probe strand contained ExBIM, the duplex containing O^6-MeG in the target strand had a higher T_m compared to when there was a G in the target strand (T_m=54.0 °C for ExBIM: O^6-MeG vs 51.7 °C for ExBIM:G, Table 1). This preference may be rationalized on the basis of more favorable hydrophobic interactions of the nucleobase analogues with the alkylated base over G, consistent with previous observations.53–58 Thus, the synthesized probes seem to discriminate between G and O^6-MeG by destabilizing the duplexes containing G.

Colorimetric discrimination of O^6-MeG in KRAS

Encouraged by the oligonucleotide duplex thermal stability data, we used oligonucleotides containing ExBenzi and ExBIM to construct AuNP-based nanoprobes targeting O^6-MeG within the KRAS sequence context. The nanoprobes were constructed by functionalizing AuNPs (d=20 nm) with thiol-modified oligonucleotides. Two types of nanoprobes were prepared: a detection nanoprobe and discriminating nanoprobes (Figure 1). The detection nanoprobe was functionalized with a 5’-thiol-modified oligonucleotide (5’-thiol_1, Table S1) with a 16-mer sequence comprised of a $(T)_{10}$ spacer and a 6-mer recognition sequence. The discriminating nanoprobes were functionalized with 17- mer oligonucleotides that were 3’-thiol-modified and consisted of a $(A)_{10}$ spacer and a 7-mer recognition sequence ending with a 5’-ExBenzi or ExBIM (3’-thiol_ExBenzi_1, 3’-thiol_ExBIM_1, respectively, Table S1). The nanoprobes were designed such that the discriminating nanoprobe (ExBenzi nanoprobe or ExBIM nanoprobe) could hybridize to the target with its 5’-tail and the

detection nanoprobe could hybridize to the target with its 3'-tail; therefore the nanoprobes were created with the capability to align in a tail-to-tail fashion in order to form a sequence complementary to the target sequences (Figure 1).

The functionalized AuNPs exhibited a characteristic surface plasmon resonance (SPR) band at 530 nm (Figure S16). In the absence of a matched target, the AuNPs remained dispersed, and the solution had a red color. When a matched target was added, it hybridized to the covalently attached probe oligonucleotides, bringing detection and discriminating nanoprobes in close proximity. Thus, a AuNP-DNA network aggregate was formed causing a change in the dielectric environment of the solution. The close proximity of the AuNPs caused a coupling of their individual localized plasmon fields and induced a red-to-purple color change that could be quantified by comparing the absorbance spectra of the solutions. Upon AuNP aggregation, the 530-nm SPR peak was red-shifted and the spectrum broadened, indicating a decrease in inter-particle distance and an increase of aggregate size (Figure S16). As a result, the absorbance at 530 nm (A_{530}) decreased while absorbance in the 700-nm (A_{700}) region increased (Figure S16). Thus, the absorbance ratio at 700 nm vs. 530 nm (A_{700}/A_{530}) is indicative of the aggregation state.59

Evaluation of thermal stability of AuNP probe:DNA aggregates

To assess the capability of the nanoprobes to distinguish between adducted and non-adducted target strands, the detection nanoprobes (1 nM) were mixed with discriminating nanoprobes containing either ExBenzi or ExBIM (1 nM). (The mixture of the detection nanoprobes with the discriminating nanoprobes containing ExBenzi or ExBIM will hereafter be referred to as ExBenzi nanoprobes and ExBIM nanoprobes, respectively). ExBenzi and ExBIM nanoprobes were supplemented with the same amount of either the O^6-MeG or G target (20 nM final concentration). Upon aggregation, the thermal stability of the aggregates was evaluated; the T_m values of the AuNP probe:target aggregates were determined by monitoring the absorbance of solutions at 530 nm (A_{530}) as a function of temperature. Increased absorbance reflects denaturation of the hybridized strands within the aggregates. The aggregates exhibited exceptionally sharp melting transitions characteristic of AuNP-DNA conjugates.60 Aggregates of the ExBenzi nanoprobes and G target had a T_m of 29.0 °C (Table 2), while those from the O^6-MeG target had a T_m of 32.0 °C (Table 2). In the case of the ExBIM nanoprobes, aggregates formed in the presence of modified target also had a higher T_m than the aggregates formed in the presence of the natural target (32.7 °C vs 29.4 °C, Table 2).

The increased discrimination achieved with the nanoprobe system is noteworthy considering that the concentration of target oligonucleotide was 110-fold lower for the nanoprobe system in comparison to the free DNA duplexes (20 nM vs 2.2 uM). The degree of discrimination (ΔT_m = *T*m probe:O^6-MeG - T_m probe:G) for ExBIM nanoprobes was 3.3 °C vs. 2.3 °C measured for the corresponding free duplexes. The sensitivity gained by incorporating the AuNPs relates to their sharp melting transitions. These are due to a combination of cooperativity of nanoparticle dissociation60 (the network of interconnected AuNPs gets progressively weaker as multiple DNA linkers dissociate) and the extremely high molar extinction coefficient of AuNPs (9×10^8 L cm^{-1} mol^{-1} for AuNPs with d= 20 nm).61

Moreover, in the nanoprobe system, the detection and discriminating nanoprobes bind to adjacent positions on the target forming a nicked DNA duplex. This design allows better mismatch discrimination from the standard DNA duplex format through cooperative hybridization of the AuNP-conjugated DNA strands to the target.

O^6-MeG recognition in mixed targets

In the aforementioned studies either methylated or undamaged DNA was targeted individually. To test whether ExBenzi and ExBIM nanoprobes could sense O^6-MeG in mixtures containing excess undamaged DNA strands we investigated the magnitude of aggregation of the nanoprobes when they were supplemented with a mixture of different targets. Solutions containing either ExBenzi (1 nM) or ExBIM nanoprobes (1 nM) were supplemented with a mixture of G target and a non-complementary 13-mer target (20 nM each, final concentration). The non-complementary target (Table S1) was included to mimic the presence of non-specific targets in the mixture. Each mixture of nanoprobes and targets was further supplemented with either 2 pmol of O^6-MeG target (20 nM final concentration) or 2 pmol of G target (40 nM final concentration). Therefore the total DNA concentration for the two supplemented solutions was equal (60 nM) but the amounts of the two competitive DNA strands were different (20 nM O^6-MeG and 20 nM G target vs 40 nM G target). Absorbance ratios (A_{700}/A_{530}) were determined in order to assess the magnitude of aggregation (Figure 3). For ExBenzi nanoprobes, aggregates from solutions supplemented with the O^6-MeG target exhibited higher A_{700}/A_{530} values than the solutions supplemented with the G target ($\Delta(A_{700}/A_{530}) = 0.31$, Figure 3). Similarly, for the ExBIM nanoprobes, aggregates from solutions supplemented with the O^6-MeG target exhibited higher A_{700}/A_{530} values than the solutions supplemented with the G target ($\Delta(A_{700}/A_{530}) = 0.36$, Figure 3). These results indicated that the selective recognition of O^6-MeG by ExBenzi or ExBIM lead to larger aggregates of the corresponding ExBenzi and ExBIM nanoprobes when mixed with the O^6-MeG target even in the presence of the competing G target.

Sensitivity of nanoprobes for detecting O^6-MeG in KRAS sequence: ExBenzi vs ExBIM nanoprobes

The sensitivity of the nanoprobes for detecting O^6-MeG in the KRAS sequence was evaluated by measuring aggregation in samples containing decreasing concentrations of the O^6-MeG target in the presence of competitive strands. Aggregates containing either the ExBenzi or ExBIM nanoprobes (1 nM each) were mixed with the G and non-complementary targets (20 nM each) and supplemented with O^6-MeG and G targets at different ratios (6 pmol in total) so that the final relative O^6-MeG concentration ([O^6-MeG]/[total DNA]) ranged from 0-13.3 % (Table S2). Upon aggregation, absorbance ratios (A_{700}/A_{530}) were measured. For both ExBenzi (Figure 4A) and ExBIM nanoprobes (Figure 4B) A_{700}/A_{530} values increased linearly as a function of the relative amount of O^6-MeG target, indicating a corresponding increase in aggregate size.

In order to compare the capability of the ExBenzi and ExBIM nanoprobes to detect O^6-MeG, we determined the limit of detection (LOD) for O^6-MeG target DNA strands (Figure 4). For the ExBenzi nanoprobes (Figure 4A) the LOD was 2.3 % O^6-MeG target or 138 fmol O^6-MeG target in the presence of 6 pmol DNA. For the ExBIM nanoprobes (Figure 4B) the

LOD was lower, namely 1.6 % O^6-MeG target or 96 fmol O^6-MeG target in the presence of 6 pmol DNA. Absorbance ratios (A_{700}/A_{530}) were also plotted as a function of the relative concentration [O^6-MeG]/[G] and corresponding standard curves appear in the Supporting Information (Figure S17). These results demonstrate that both ExBenzi and ExBIM nanoprobes, can be used for the competitive quantitative detection of O^6-MeG, with ExBIM being approximately 1.4-fold more sensitive in the tested sequence context, and that they are effective in the presence of G target DNA strands even when O^6-MeG target is a minor component of the mixture.

It is notable that the nanoprobes distinguish the presence of a single methyl group in one of the 13 bases of a target strand, and that the selection is achieved without heating and under non-stringent salt conditions, which are often needed for mismatch discrimination for single nucleotide polymorphism (SNP) detection. A feature of these nanoprobes that suggests their further potential in bioanalytical applications is their compatibility with AuNP-based techniques currently used for SNP detection in unamplified genomic samples.62–66 In this study, the increase in AuNP aggregation associated with the presence of the O^6-MeG target was monitored by UV-Vis spectroscopy. It can be anticipated that with further engineering, the adduct-sensitive AuNP aggregation could be monitored with analytical readouts that are significantly more sensitive than absorbance, such as light-scattering,65,66 scanometric62,64 or electrical detection63 currently applied for SNP detection in unamplified genomic samples.

Data from melting studies of the DNA duplexes, as well as AuNP-DNA aggregates, together with data from the colorimetric ratiometric detection studies suggest that both ExBenzi and ExBIM have a higher affinity for O^6-MeG than for G. The relative performance of the two novel nucleoside analogues is compared in Table S3. In duplex DNA, there appears to be a slight increase in discrimination in the case of ExBenzi, whereas the detection capacity of the nanoprobe system is slightly improved in the case of ExBIM. The similarity between the two analogues suggest a lack of relevant hydrogen bonding interactions between the adduct and probes since the analogues differ only in H-bonding capacity. From a synthetic perspective, however, ExBIM can be produced with consistently higher yields primarily due to better solubility characteristics during work-up and purification.

Detection of O^6-MeG oligonucleotide targets in the presence of human genomic DNA

We investigated the performance of the ExBIM nanoprobes for detecting O^6-MeG oligonucleotide targets in the presence of human genomic DNA. Genomic DNA extracted from SW480 colon carcinoma cells was fragmented by ultrasonication (Figure S18). ExBIM nanoprobes (1 nM) were combined with fragmented genomic DNA (100 ng) and O^6-MeG oligonucleotides. The same target sequence with G at the modification position was also added as a direct competitor. Ratios of added O^6-MeG to G targets where the same as when the sensitivity of the nanoprobes was assessed with non-complementary oligonucleotides as background. The final relative concentration of O^6-MeG in the sample ([O^6-MeG]/[total DNA]) ranged from 0-2.8 % (Table S4). Upon target-induced aggregation, absorbance ratios (A_{700}/A_{530}) were measured. Ratiometric absorbance values A_{700}/A_{530} increased linearly as a function of O^6-MeG target concentration (Figure 5), indicating a corresponding increase in

aggregation. The LOD for O^6-MeG DNA strands with genomic DNA as background (Figure 5) was 0.24 %, indicating that the presence of a large background of fragmented genomic DNA did not interfere with the sensing response of the nanoprobes and quantification of O^6-MeG.

Specificity of ExBIM nanoprobes

The specificity of ExBIM towards O^6-MeG as opposed to adducts containing other alkyl groups on the O^6-position of guanine was also examined. ExBIM nanoprobes (1 nM) were mixed with the same amount (20 nM, final concentration) of a 13-mer KRAS sequence target that contained either O^6-MeG or O^6-BnG at the middle position (O^6-BnG_13mer target, Table S1). The color of the O^6-MeG-supplemented suspension turned purple, whereas the color of the O^6-BnG-supplemented suspension remained red (Figure S19). This observation suggested that the O^6-BnG target did not induce any aggregation. To further confirm the accuracy of this simple visual observation, the solutions were gradually heated and A_{530} was monitored as a function of temperature. Characteristic sharp melting transitions were observed for O^6-MeG whereas the A_{530} did not change for O^6-BnG, further indicating the absence of aggregates and confirming the naked-eye inspection (Figure S20). These results indicate a lack of affinity of ExBIM for O^6-BnG. Furthermore, the convenience of visually judging aggregation due to color changes associated with the SPR phenomenon suggests a future utility of the assay for screening diverse analogues with the goal of optimizing base surrogates for selection toward different DNA adducts.

Effect of target length

Hypothesizing that longer target sequences would result in lower discrimination, we investigated thermal stability differences for longer DNA duplexes containing ExBIM placed opposite either O^6-MeG or G. Therefore, we synthesized longer target oligonucleotides (17 and 21-mer) for which the middle base of the target was the middle base of KRAS codon 13 (Figure 2) and contained in the middle position either O^6-MeG or G (Table S1). The corresponding complementary probe oligonucleotides containing ExBIM in the middle position were also synthesized (Table S1) and the T_m of the DNA duplexes formed from the probe and target strands was determined. For the 17-mer DNA duplex the ΔT_m was 1.6 °C (Table S5). For the 21-mer duplex the ΔT_m was 1.3 °C (Table S5). It should be noted that the melting analysis experiments for the longer targets (17 and 21-mer) were performed with a lower DNA concentration (1 uM) than for the 13-mer targets (2.2 uM) to ensure that the A260 measurements were in the linear response range of the UV/Vis spectrophotometer.

To test the capability of ExBIM to distinguish between O^6-MeG and G in longer DNA strands using nanoprobes, we prepared detection and discriminating ExBIM nanoprobes designed to hybridize with either the 17-mer or 21-mer KRAS codon 13 targets. Thus, the same type of AuNPs (d=20 nm) were functionalized with longer 5'-thiolated oligonucleotides (5'-thiol_2 and 5'-thiol_3, Table S1) to yield detection nanoprobes targeting the 17- and 21-mer target, respectively. Similarly, discriminating ExBIM nanoprobes were produced by functionalizing AuNPs with longer 3'-thiolated oligonucleotides (3'-thiol_ExBIM_2 and 3'-thiol_ExBIM_3, Table S1). The detection and discriminating ExBIM nanoprobes (1 nM each) were mixed with the same amount (20 nM

final concentration) of either O^6-MeG or G target, and the T_m values for the resulting aggregates were determined. For the 17-mer target, aggregates formed in the presence of O^6-MeG target exhibited a higher T_m than the aggregates formed in the presence of G target (47.7 °C for O^6-MeG vs 44.1 °C for G, ΔT_m= 3.6 °C, Table S6). Similarly, for the 21- mer target, aggregates formed in the presence of O^6-MeG exhibited a higher T_m than aggregates formed from the ExBIM nanoprobes and G target (62.0 °C for O^6-MeG vs 60.2 °C for G, ΔT_m= 1.8 °C, Table S6). The thermal stability of AuNP-DNA aggregates is influenced by the interparticle distance, which is modulated by a combination of the length of the interconnecting oligonucleotides and efficiency of hybridization. Hybridization efficiency, in turn, is influenced by the ratio of mismatched to matched bases. Thus, as hypothesized, discrimination diminished for the longest target. However, balancing the combination of interparticle distance and hybridization efficiency influences, discrimination for the 17-mer target was no worse than for the 13-mer. The 17-mer target was therefore preferred for further studies because there was no loss in discrimination.

Detection of O^6-MeG in KRAS cod12

To address the potential influence of sequence context, ExBIM nanoprobes targeting KRAS codon 12 were also developed. Thus, 17-mer target oligonucleotides in which the middle base (either O^6-MeG or G) was the middle base of KRAS codon 12 were synthesized (Figure 2, Table S7). Aggregates formed between KRAS codon 12-targeting nanoprobes in the presence of the O^6-MeG target (20 nM final concentration) exhibited a higher T_m than those formed in the presence of the G target (ΔT_m = 2.0 °C). These results indicate that ExBIM can also discriminate between O^6-MeG and G in targets with different sequence context.

In conclusion, the design, synthesis, and incorporation of the novel nucleoside analogues ExBenzi and ExBIM into DNA hybridization probes are reported in this study. Both of the novel probes have a higher affinity for O^6-MeG than for G in DNA duplexes containing sequences of cancer-related mutational hotspots. Hybridization probes containing ExBenzi and ExBIM were coupled to AuNPs. These were the basis of a method for the sequence-specific quantification of DNA strands containing O^6-MeG in the presence of different competitor strands and human genomic DNA. To the best of our knowledge, this is the first sensing strategy for in-gene quantification of the highly mutagenic DNA adduct O^6-MeG in a complex mixture. Studies to elucidate the molecular origin of discrimination of O^6-MeG from G by ExBIM and ExBenzi on the basis of their orientation in DNA and stacking capacity are anticipated. Finally, integration of the nanoprobes developed in this study with hybrid capture techniques regularly used for targeted enrichment of nucleic acids prior to next generation sequencing and with well-established ultrasensitive AuNP-based DNA detection technologies used for SNP detection in unamplified genomic samples may enable monitoring the in-gene abundance of O^6-MeG in biological samples.

Supplementary Material

Refer to Web version on PubMed Central for supplementary material.

Acknowledgment

This work was supported ba the European Research Council (260341 and 680920) and the Swiss national Science Foundation (31003A_156280). We thank Larissa Roth for synthesizing oligonucleotides and for performing DNA duplex melting analyses. We thank Dr. Laura Wyss for helping with the synthesis of phosphoramidites and writing.

Funding Sources

This work was supported by the European Research Council (260341) and the Swiss National Science Foundation (31003A_156280).

References

(1). Kyrtopoulos SA, Ampatzi P, Davaris P, Haritopoulos N, Golematis B. Carcinogenesis. 1990; 11:431. [PubMed: 2311187]

(2). Kyrtopoulos SA. Mutat Res Fundam Mol Mech Mutagen. 1998; 405:135.

(3). Mirvish SS. Cancer Lett. 1995; 93:17. [PubMed: 7600541]

(4). Rydberg B, Lindahl T. EMBO J. 1982; 1:211. [PubMed: 7188181]

(5). Harrison KL, Jukes R, Cooper DP, Shuker DEG. Chem Res Toxicol. 1999; 12:106. [PubMed: 9894025]

(6). Sedgwick B. Carcinogenesis. 1997; 18:1561. [PubMed: 9276631]

(7). Abbott PJ, Saffhill R. Biochim Biophys Acta Nucleic Acids Protein Synth. 1979; 562:51.

(8). Saffhill R, Hall JA. Chem-Biol Interact. 1985; 56:363. [PubMed: 4075456]

(9). Saffhill R, Margison GP, O'Connor PJ. Biochim Biophys Acta Rev Cancer. 1985; 823:111.

(10). Rossi SC, Conrad M, Voigt JM, Topal MD. Carcinogenesis. 1989; 10:373. [PubMed: 2643488]

(11). O'Reilly SM, Newlands ES, Brampton M, Glaser MG, Rice-Edwards JM, Illingworth RD, Richards PG, Kennard C, Colquhoun IR, Lewis P, Stevens MFG. Eur J Cancer. 1993; 29:940.

(12). Mirsalis JC, Monforte JA, Winegar RA. Crit Rev Toxicol. 1994; 24:255. [PubMed: 7945893]

(13). Pegg AE. Cancer Res. 1990; 50:6119. [PubMed: 2205376]

(14). Foiles PG, Miglietta LM, Akerkar SA, Everson RB, Hecht SS. Cancer Res. 1988; 48:4184. [PubMed: 3390812]

(15). Kang, H-i, Konishi, C., Kuroki, T., Huh, N-h. Carcinogenesis. 1995; 16:1277. [PubMed: 7788843]

(16). Kang H, Konishi C, Kuroki T, Huh N. Environ Health Perspect. 1993; 99:269. [PubMed: 8319641]

(17). Kang H, Konishi C, Eberle G, Rajewsky MF, Kuroki T, Huh N. Cancer Res. 1992; 52:5307. [PubMed: 1394135]

(18). Georgiadis P, Kaila S, Makedonopoulou P, Fthenou E, Chatzi L, Pletsa V, Kyrtopoulos SA. Cancer Epidemiol Biomarkers Prev. 2011; 20:82. [PubMed: 21081711]

(19). vanDelft JHM, Steenwinkel M, deGroot AJL, vanZeeland AA, EberleAdamkiewicz G, Rajewsky MF, Thomale J, Baan RA. Fundam Appl Toxicol. 1997; 35:131. [PubMed: 9024680]

(20). Brink A, Lutz U, Volkel W, Lutz WK. J Chromatogr B. 2006; 830:255.

(21). Pfeifer GP, Drouin R, Holmquist GP. Mutat Res Fundam Mol Mech Mutagen. 1993; 288:39.

(22). Tornaletti, S., Pfeifer, G. Technol Detect DNA Damage Mutat. Pfeifer, G., editor. Springer; US: 1996. p. 199

(23). Cloutier J-F, Drouin R, Castonguay A. Chem Res Toxicol. 1999; 12:840. [PubMed: 10490506]

(24). Cloutier J-F, Drouin R, Weinfeld M, O'Connor TR, Castonguay A. J Mol Biol. 2001; 313:539. [PubMed: 11676538]

(25). Clark T, Spittle K, Turner S, Korlach J. Genome Integr. 2011; 2:10. [PubMed: 22185597]

(26). Riedl J, Ding Y, Fleming AM, Burrows CJ. Nat Commun. 2015:6.

(27). Riedl J, Fleming AM, Burrows CJ. J Am Chem Soc. 2016; 138:491. [PubMed: 26741640]

(28). Onizuka K, Nishioka T, Li Z, Jitsuzaki D, Taniguchi Y, Sasaki S. Chem Commun. 2012; 48:3969.

(29). Gong J, Sturla SJ. J Am Chem Soc. 2007; 129:4882. [PubMed: 17402738]

(30). Gahlon HL, Sturla SJ. Chem Eur J. 2013; 19:11062. [PubMed: 23801518]
(31). Angelov T, Dahlmann HA, Sturla SJ. Bioorg Med Chem. 2013; 21:6212. [PubMed: 23969036]
(32). Wyss LA, Nilforoushan A, Eichenseher F, Suter U, Blatter N, Marx A, Sturla SJ. J Am Chem Soc. 2015; 137:30. [PubMed: 25490521]
(33). Nilforoushan A, Furrer A, Wyss LA, van Loon B, Sturla SJ. J Am Chem Soc. 2015; 137:4728. [PubMed: 25786104]
(34). Gahlon HL, Schweizer WB, Sturla SJ. J Am Chem Soc. 2013; 135:6384. [PubMed: 23560524]
(35). Sturla SJ. Curr Opin Chem Biol. 2007; 11:293. [PubMed: 17574899]
(36). Trantakis IA, Sturla SJ. Chem Commun. 2014; 50:15517.
(37). Guckian KM, Schweitzer BA, Ren RX, Sheils CJ, Tahmassebi DC, Kool ET. J Am Chem Soc. 2000; 122:2213. [PubMed: 20865137]
(38). Guckian KM, Schweitzer BA, Ren RXF, Sheils CJ, Paris PL, Tahmassebi DC, Kool ET. J Am Chem Soc. 1996; 118:8182. [PubMed: 20882117]
(39). Lu H, He K, Kool ET. Angew Chem Int Ed. 2004; 43:5834.
(40). Gao J, Liu H, Kool ET. J Am Chem Soc. 2004; 126:11826. [PubMed: 15382917]
(41). Liu H, Gao J, Kool ET. J Org Chem. 2005; 70:639. [PubMed: 15651812]
(42). Lee AHF, Kool ET. J Org Chem. 2005; 70:132. [PubMed: 15624915]
(43). Kowal EA, Lad RR, Pallan PS, Dhummakupt E, Wawrzak Z, Egli M, Sturla SJ, Stone MP. Nucleic Acids Res. 2013; 41(15):7568.
(44). Kidwai M, Saxena S, Mohan R. J Heterocycl Chem. 2005; 42:703.
(45). Herbert JM, Woodgate PD, Denny WA. J Med Chem. 1987; 30:2081. [PubMed: 3669016]
(46). Sachs F. Liebigs Ann Chem. 1909; 365:53.
(47). Hansen AS, Thalhammer A, El-Sagheer AH, Brown T, Schofield CJ. Bioorg Med Chem Lett. 2011; 21:1181. [PubMed: 21256007]
(48). Lakshman MK, Zajc B. Nucleosides Nucleotides. 1996; 15:1029.
(49). Bleasdale C, Ellwood SB, Golding BT. J Chem Soc Perk T 1. 1990:803.
(50). Arrington AK, Heinrich EL, Lee W, Duldulao M, Patel S, Sanchez J, Garcia-Aguilar J, Kim J. Int J Mol Sci. 2012; 13:12153. [PubMed: 23202889]
(51). Leonard GA, Thomson J, Watson WP, Brown T. Proc Natl Acad Sci U S A. 1990; 87:9573. [PubMed: 2263612]
(52). Wong C-W, Tan N-W, Li BFL. J Mol Biol. 1992; 228:1137. [PubMed: 1474583]
(53). Ogawa AK, Wu Y, McMinn DL, Liu J, Schultz PG, Romesberg FE. J Am Chem Soc. 2000; 122:3274.
(54). Wu Y, Ogawa AK, Berger M, McMinn DL, Schultz PG, Romesberg FE. J Am Chem Soc. 2000; 122:7621.
(55). Brotschi C, Häberli A, Leumann CJ. Angew Chem Int Ed. 2001; 40:3012.
(56). Kool ET, Morales JC, Guckian KM. Angew Chem Int Ed. 2000; 39:990.
(57). O'Neill BM, Ratto JE, Good KL, Tahmassebi DC, Helquist SA, Morales JC, Kool ET. J Org Chem. 2002; 67:5869. [PubMed: 12182615]
(58). Guckian KM, Morales JC, Kool ET. J Org Chem. 1998; 63:9652. [PubMed: 20852720]
(59). Trantakis IA, Bolisetty S, Mezzenga R, Sturla SJ. Langmuir. 2013; 29:10824. [PubMed: 23883185]
(60). Storhoff JJ, Elghanian R, Mucic RC, Mirkin CA, Letsinger RL. J Am Chem Soc. 1998; 120:1959.
(61). Liu X, Atwater M, Wang J, Huo Q. Colloids Surf B. 2007; 58:3.
(62). Bao YP, Huber M, Wei TF, Marla SS, Storhoff JJ, Muller UR. Nucleic Acids Res. 2005:33.
(63). Park S-J, Taton TA, Mirkin CA. Science. 2002; 295:1503. [PubMed: 11859188]
(64). Taton TA, Mirkin CA, Letsinger RL. Science. 2000; 289:1757. [PubMed: 10976070]
(65). Storhoff JJ, Lucas AD, Garimella V, Bao YP, Müller UR. Nat Biotechnol. 2004; 22:883. [PubMed: 15170215]

Europe PMC Funders Author Manuscripts

(66). Storhoff JJ, Marla SS, Bao P, Hagenow S, Mehta H, Lucas A, Garimella V, Patno T, Buckingham W, Cork W, Müller UR. Biosens Bioelectron. 2004; 19:875. [PubMed: 15128107]

Europe PMC Funders Author Manuscripts

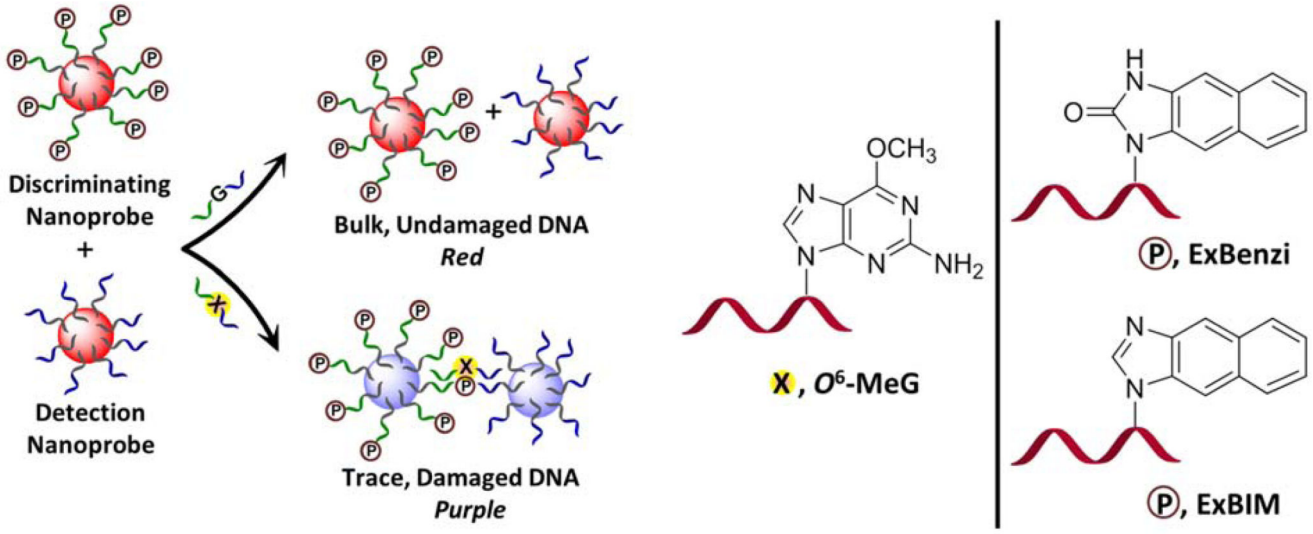

Figure 1.

Schematic representation of the nanoprobe-based detection of the highly mutagenic O^6-MeG. The novel synthetic nucleosides ExBenzi and ExBIM lead to the formation of more stable DNA duplexes when they are paired with O^6-MeG than with G. Gold nanoparticles (AuNPs) functionalized with ordinary oligonucleotides serve as detection nanoprobes while AuNPs functionalized with oligonucleotides containing a synthetic nucleoside (indicated by terminal P) serve as discriminating nanoprobes. In the presence of O^6-MeG target DNA strands, the detection nanoprobes can align in a tail-to-tail fashion with the discriminating nanoprobes. The hybridization of the target leads to aggregation of AuNPs accompanied by a change in the color of the solution from red to purple.

Europe PMC Funders Author Manuscripts

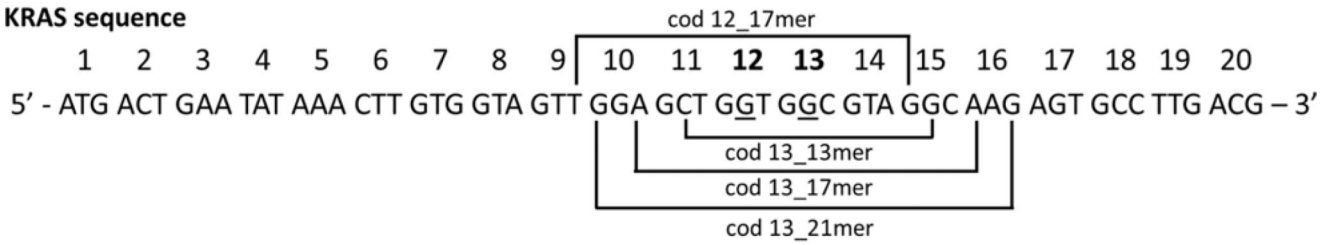

Figure 2.

KRAS gene sequence studied herein. The target oligonucleotides were designed such that their middle base was the middle base of either codon 12 or codon 13 (underlined bases). The length of the targets was varied for the evaluation studies performed with targets centered on codon 13 (13-, 17-, 21-mer). The target was a 17-mer for the codon 12-based studies.

Europe PMC Funders Author Manuscripts

Europe PMC Funders Author Manuscripts

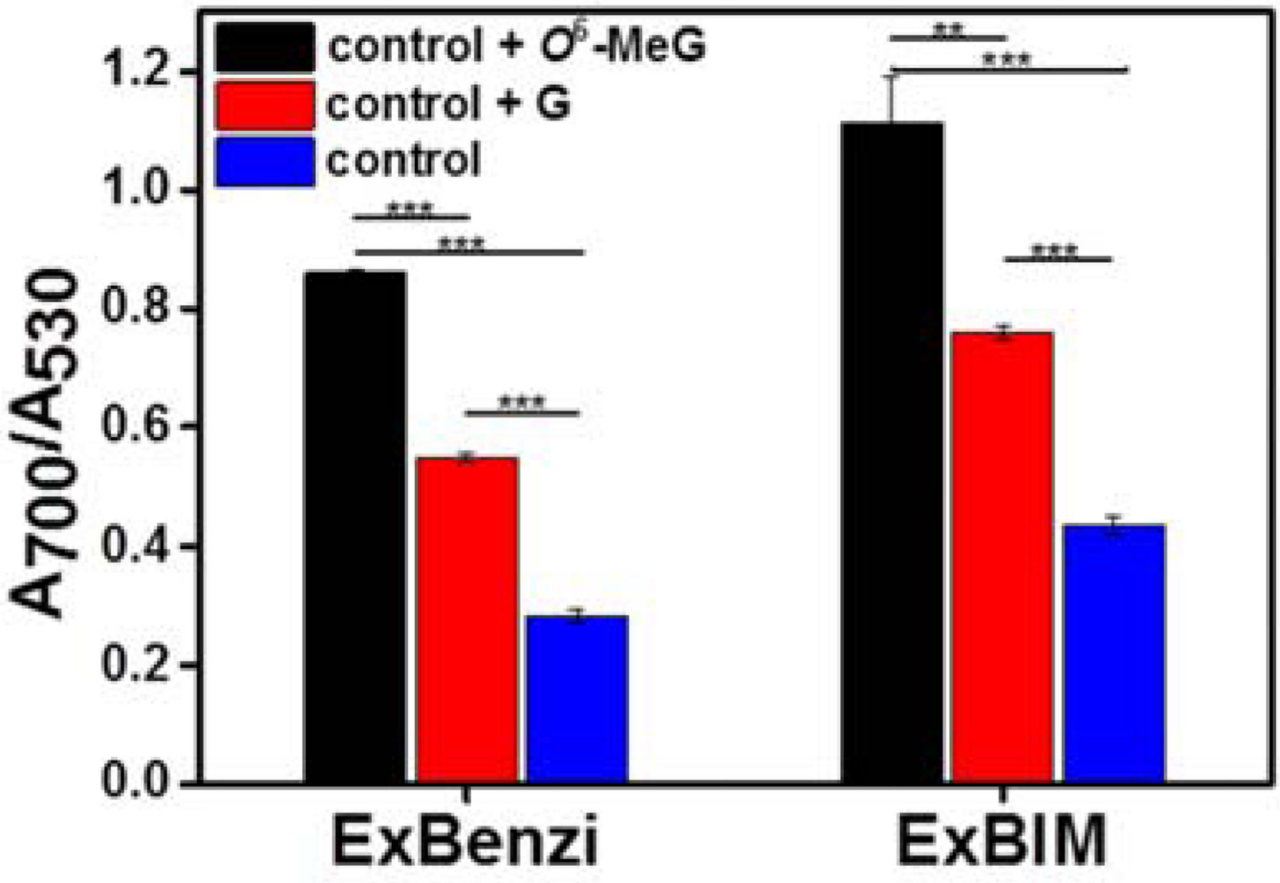

Figure 3.

Absorbance ratios of aggregates formed from ExBenzi or ExBIM nanoprobes and target mixtures (20 nM of each G and non-complementary target, control) supplemented with either the O^6-MeG (control + O^6-MeG, 20 nM final concentration) or G target (control + G, 40 nM final concentration). Aggregates formed from the initial mixture (control) served as the control. Data are mean±SD from three independent experiments. Significant differences indicated as ** for $P<0.01$ and *** for $P<0.001$.

Europe PMC Funders Author Manuscripts

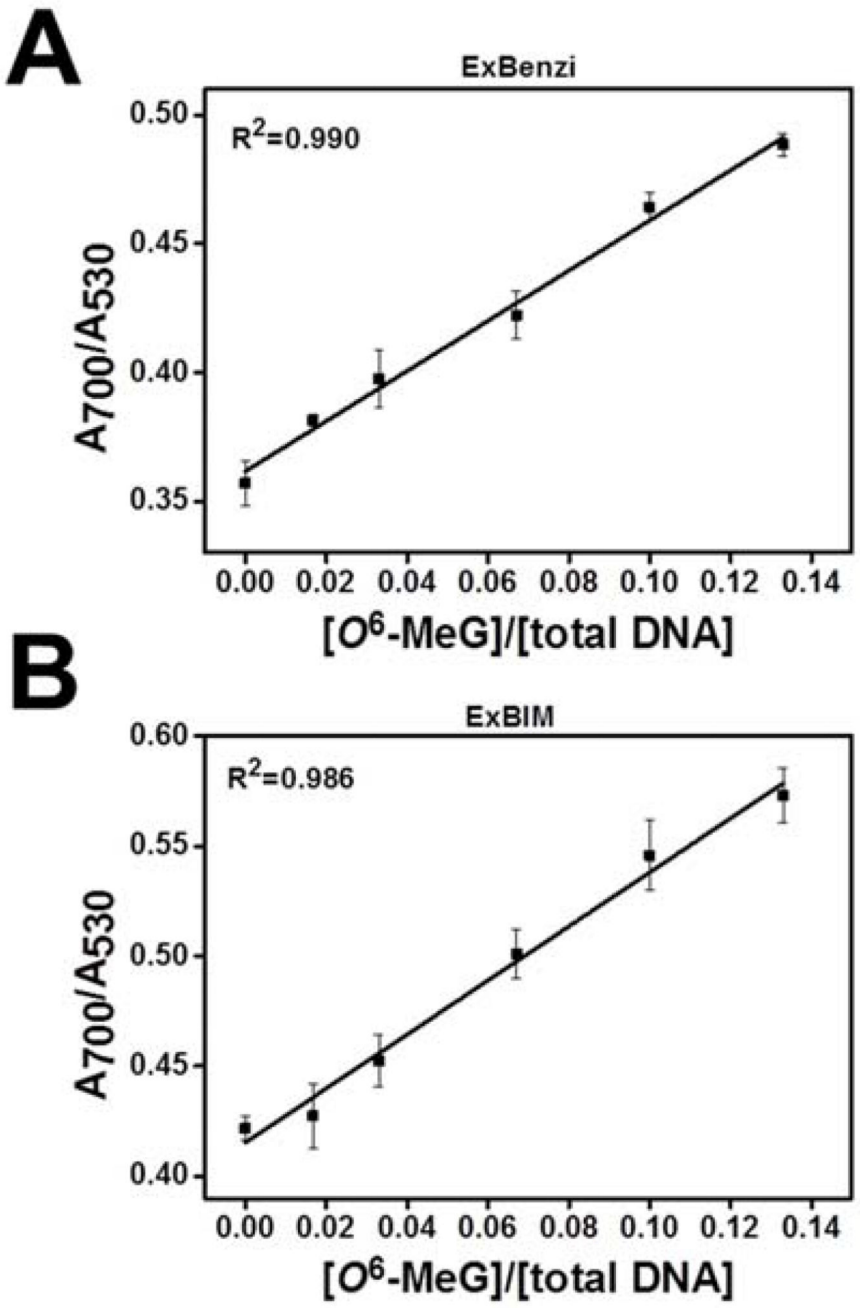

Figure 4.

Absorbance ratios (A_{700}/A_{530}) as a function of relative O^6-MeG target concentrations ([O^6-MeG] / [total target DNA] for aggregates formed from (A) ExBenzi or (B) ExBIM nanoprobes. Data points indicate mean ± SD from three independent experiments.

Europe PMC Funders Author Manuscripts

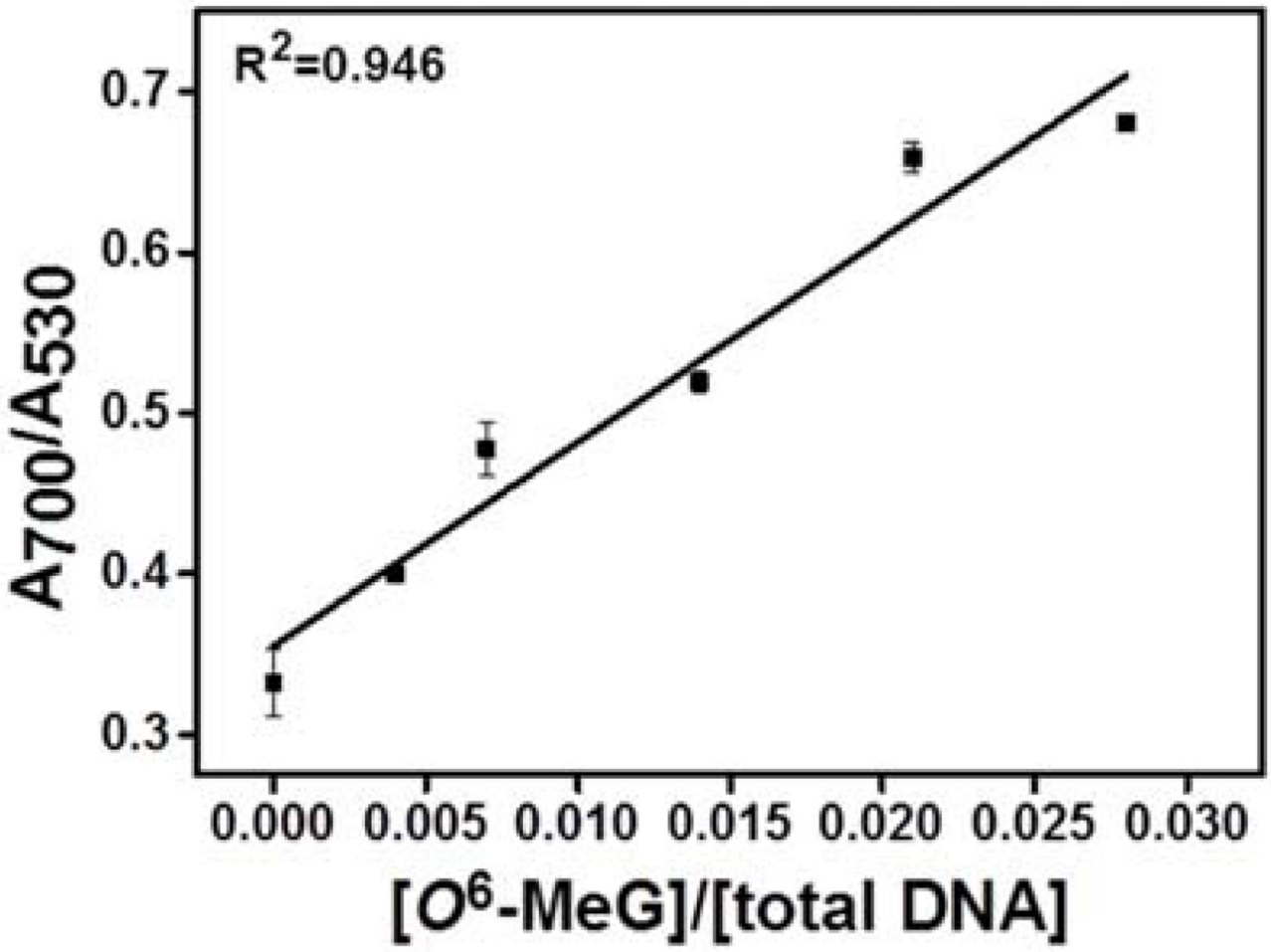

Figure 5.

Absorbance ratios (A_{700}/A_{530}) as a function of relative O^6-MeG target concentrations ([O^6-MeG] / [total target DNA] for aggregates formed from ExBIM nanoprobes in the presence of fragmented human genomic DNA. Data points indicate mean±SD from three independent experiments.

Europe PMC Funders Author Manuscripts

Table 1

Melting temperatures of 13-mer DNA duplexes centered on KRAS codon 13 in which the target strand contains in the middle position either G or O^6-MeG and the base in the middle position of the complementary strand is C, ExBenzi, or ExBIM.

Paired bases	T_m(°C)	ΔT_m(°C)[a]
C:G C:O^6-MeG	66.0±0.6 55.2±0.2	-10.8±0.6
ExBenzi:G ExBenzi: O^6-MeG	52.0±0.7 55.0±0.7	+3.0±1.0
ExBIM:G ExBIM: O^6-MeG	51.7±0.6 54.0±1.0	+2.3±1.2

[a] $\Delta T_m = T_m(O^6\text{-MeG duplex}) - T_m(\text{G duplex})$

[b] Data are mean ± SD from three independent experiments

Europe PMC Funders Author Manuscripts

Table 2

Melting temperatures of AuNP aggregates formed by either the ExBenzi or ExBIM nanoprobes and the 13-mer KRAS codon 13 target (containing either O^6-MeG or G in the middle position).

Paired bases	T_m(°C)	ΔT_m(°C)[a]
ExBenzi:G ExBenzi: O^6-MeG	29.0±0.0 32.0±0.0	+3.0±0.0
ExBIM:G ExBIM: O^6-MeG	29.4±0.6 32.7±0.6	+3.3±0.8

[a] $\Delta T_m = T_m(O^6\text{-MeG aggregates}) - T_m(\text{G aggregates})$

[b] Data are mean ± SD from three independent experiments